J Electroceram (2012) 29:29–36
DOI 10.1007/s10832-012-9734-3

Electrical conductivities of strontium-doped rare earth ultraphosphates and oxyphosphates

Atsushi Unemoto · Koji Amezawa · Tatsuya Kawada

Received: 14 January 2012 / Accepted: 30 April 2012 / Published online: 13 May 2012

Abstract Electrical conductivity of lanthanum ultraphosphate and neodymium oxyphosphate both doped with strontium, $La_{1-x}Sr_xP_5O_{14-\delta}$ (x=0, 0.01, 0.03 and 0.05 in nominal formulae) and $(Nd_{1-x}Sr_x)_3PO_{7-\delta}$ (x=0 and 0.03), respectively, was investigated with a two-probe ac technique. The electrical conductivity was measured as functions of oxygen partial pressure and water vapor pressure in the temperature range of 523 to 673 K for the former and 973 to 1273 K for the latter. $La_{1-x}Sr_xP_5O_{14-\delta}$ have considerable protonic conductivity, which was evidenced by isotope effect of hydrogen and deuteron on the electrical conductivity, over the wide range of oxygen partial pressure such as oxygen and hydrogen containing atmospheres. $La_{1-x}Sr_xP_5O_{14-\delta}$ exhibit protonic conductivities of 4.7×10^{-5}–2.2×10^{-3} S cm^{-1} in the temperature range of 523–673 K, which is comparable to the other phosphate based protonic conductors. Although protonic defects are considered to be induced and a major positive defect in $(Nd_{0.97}Sr_{0.03})_3PO_{7-\delta}$, attributed to small protonic mobility, $(Nd_{0.97}Sr_{0.03})_3PO_{7-\delta}$ is a mixed oxide ion and electron hole conductor at 1173–1273 K, then, it turns to be electron hole conductor below temperatures of 1073 K. $(Nd_{0.97}Sr_{0.03})_3PO_{7-\delta}$ in 1.0×10^{-2} atm oxygen–1.9×10^{-2} atm water vapor had smaller conductivity than that in unhumidified 1.0×10^{-2} atm oxygen. The conductivities were 9.7×10^{-3}–3.1×10^{-1} S cm^{-1} and 2.8×10^{-3}–2.5×10^{-1} S cm^{-1} in the above gases, respectively, in the temperature range of 973–1273 K. $(Nd_{0.97}Sr_{0.03})_3PO_{7-\delta}$ had larger activation energy such as 165 kJ mol^{-1} than proton conducting $La_{1-x}Sr_xP_5O_{14-\delta}$ (76 kJ mol^{-1}) including other proton conducting phosphates (68–86 kJ mol^{-1}).

Keywords Lanthanum ultraphosphate · Neodymium oxyphosphate · Defects · Conductivity

A. Unemoto (✉)
Institute of Multidisciplinary Research for Advanced Materials,
Tohoku University,
2-1-1 Katahira, Aoba-ku,
Sendai 980-8577, Japan
e-mail: unemoto@tagen.tohoku.ac.jp

K. Amezawa · T. Kawada
Graduate School of Environmental Studies, Tohoku University,
6-6 Aoba, Aramaki, Aoba-ku,
Sendai 980-8579, Japan

1 Introduction

Some acceptor-doped ceramics such as perovskite-type oxides [1–10], phosphates [11–26], borates [27], niobates and tantalates [28] etc. are known to significantly conduct protons at high temperatures. For such materials, oxygen deficiency and ambient water vapor are essential in order to exhibit protonic conductivity. In the case of $(La,Sr)PO_4$, for instance, substitution of lower valent cation, Sr in this case, into La-site leads to the formation of oxygen deficiency. The formation of oxygen deficiency accompanied by dopant dissolution is expressed [13] by using the Kröger-Vink notation [29] as,

$$\frac{1}{2}Sr_2P_2O_7 \rightarrow Sr'_{La} + \frac{1}{2}(P_2O_7)^{\bullet\bullet}_{2PO_4} \quad (1)$$

The equilibrium of the ceramics with water vapor can be written as,

$$\frac{1}{2}(P_2O_7)^{\bullet\bullet}_{2PO_4} + \frac{1}{2}H_2O \underset{\leftarrow}{\rightarrow} (HPO_4)^{\bullet}_{PO_4} \quad (2)$$

The carrier concentration in the material can be expressed using the equilibrium constant, K_1, of Eq. (2) as,

$$\left[(HPO_4)^{\bullet}_{PO_4}\right] = K_1\left[(P_2O_7)^{\bullet\bullet}_{2PO_4}\right]^{\frac{1}{2}} p_{H_2O}^{\frac{1}{2}} \quad (3)$$

High-temperature protonic conductors are expected as candidates of the electrolytes for electrochemical devices such as gas sensors, hydrogen pumps, steam electrolysis

and solid oxide fuel cells [3–7]. Especially for solid oxide fuel cell application, intermediate temperature operation such as 673–873 K is advantageous because the activation energy of proton migration is generally smaller than that of oxide ion migration [6, 7]. However, some of the proton conducting ceramics developed earlier, i.e. cerates, are highly reactive to ambient gases such as carbon dioxide and/or water vapor [30–35], since they contain alkaline earth metals as a main component. Thus, one of the important scientific and technological challenges is to let the ceramics have high chemical stabilities against the abovementioned gas species while having high protonic conductivity. In this context, rare-earth phosphates, which do not contain the alkaline earth metals as main component, are expected as one of material candidates showing high chemical stabilities as well as high protonic conductivity.

To date, phase relationships of La_2O_3–P_2O_5 and Nd_2O_3–P_2O_5 were revealed by Niinisto and Keskela [36], and Wong and Kreidler [37], respectively. Both systems have RE_3PO_7, $RE_7P_3O_{18}$, $REPO_4$, REP_3O_9, $RE_2P_4O_{13}$ and REP_5O_{14} (RE=La, Nd). In this study, we chose lanthanum ultraphosphate, $(La,Sr)P_5O_{14}$, and neodymium oxyphosphate, $(Nd,Sr)_3PO_7$, as target materials for evaluation of the electrical conductivities. So far, preparation methods of the rare-earth ultraphosphates [38, 39], crystal structural analysis [40, 41], luminescent properties of the rare-earth oxyphosphates [42–44], and recently electrical conductivity of non-dope LaP_5O_{14} [25, 26] and a single crystal of Sr-doped LaP_5O_{14} [26] have been investigated. However, there still remain questions on the correlation between the defect structure and the electrical conductivities for both phosphates. Since the defect structure, thus the electrical conductivity, is affected by the gas partial pressures, the electrical conductivity is needed to be investigated under controlled environments, i.e. oxygen partial pressure and water vapor pressure, in order to achieve better understanding the defect structures and the conducting natures.

As mentioned in the 1st paragraph of this section, the oxygen deficit in the lanthanum ortho-phosphates is introduced as $(P_2O_7)^{\bullet\bullet}_{2PO_4}$ by Sr-doping into La-site as in Eq. (1) [13]. In the cases of the lanthanum ultraphosphates and neodymium oxyphosphates, however, it is not sure how the oxygen deficit is introduced. Thus, for convenience, we use $V_O^{\bullet\bullet}$ to express the oxygen deficit for the following. The oxygen deficit is induced by doping of Sr into La-site and Nd-site of ultraphosphates and oxyphosphates, respectively, as,

$$SrO \rightarrow Sr'_{RE} + O_O^{\times} + \frac{1}{2}V_O^{\bullet\bullet} \tag{4}$$

The equilibrium of the ultraphosphate and oxyphosphate with oxygen gas is expressed as,

$$\frac{1}{2}O_2 + V_O^{\bullet\bullet} = O_O^{\times} + 2h^{\bullet} \tag{5}$$

and the equilibrium constant, K_2, of Eq. (4),

$$K_2 = \frac{\left[O_O^{\times}\right]\left[h^{\bullet}\right]^2}{p_{O_2}^{\frac{1}{2}}\left[V_O^{\bullet\bullet}\right]} \tag{6}$$

The equilibrium of the ceramics with ambient water vapor is expressed as,

$$H_2O + O_O^{\times} + V_O^{\bullet\bullet} = 2(OH)_O^{\bullet} \tag{7}$$

The equilibrium constant, K_3, of Eq. (6),

$$K_3 = \frac{\left[(OH)_O^{\bullet}\right]^2}{p_{H_2O}\left[O_O^{\times}\right]\left[V_O^{\bullet\bullet}\right]} \tag{8}$$

The charge neutrality condition provides,

$$\left[(OH)_O^{\bullet}\right] + 2\left[V_O^{\bullet\bullet}\right] + \left[h^{\bullet}\right] = \left[Sr'_{La}\right] \tag{9}$$

The site balance of O^{2-}-site gives,

$$\left[O_O^{\times}\right] + \left[V_O^{\bullet\bullet}\right] + \left[(OH)_O^{\bullet}\right] = 3 \tag{10}$$

Based on Eqs. (6), (8)–(10), the oxygen partial pressure and water vapor pressure dependences of the defect concentrations are shown in Fig. 1 (a) and (b), respectively.

The total conductivity, σ, is expressed by sum of the partial conductivity contributions of species i as,

$$\sigma = \sigma_{H^+} + \sigma_{O^{2-}} + \sigma_h \tag{11}$$

The partial conductivity is related to the defect concentration of species i as,

$$\sigma_i = z_i e m_i c_i \tag{12}$$

where z_i, m_i and c_i are the charge number, the mobility and the concentration of species i. e is the elementary charge. From the gas partial pressure dependence of the electrical conductivity, predominant carriers can be estimated under the assumption that the mobility is independent of gas partial pressures. For instance, when the charge neutrality condition, $\left[Sr'_{Nd}\right] = 2\left[V_O^{\bullet\bullet}\right]$, holds, the concentrations of proton and electron hole are expressed as $\left[(OH)_O^{\bullet}\right] \propto p_{H_2O}^{\frac{1}{2}}$ and $[h] \propto p_{O_2}^{\frac{1}{4}}$, respectively. Thus, the partial conductivities of oxide ion, proton and electron hole are expressed as, $\sigma_{O^{2-}} = \sigma^{\circ}_{O^{2-}}$, $\sigma_{H^+} = \sigma^{\circ}_{H^+} p_{H_2O}^{\frac{1}{2}}$ and $\sigma_h = \sigma^{\circ}_h p_{O_2}^{\frac{1}{4}}$, respectively, where $\sigma^{\circ}_{O^{2-}}$, $\sigma^{\circ}_{H^+}$ and σ°_h are constants. Similarly, when the electron hole is the major positive defects, i.e. $\left[Sr'_{Nd}\right] = [h]$, the relations, $\sigma_{O^{2-}} = \sigma^{\circ}_{O^{2-}} p_{O_2}^{-\frac{1}{2}}$, $\sigma_{H^+} = \sigma^{\circ}_{H^+} p_{O_2}^{-\frac{1}{4}} p_{H_2O}^{\frac{1}{2}}$ and

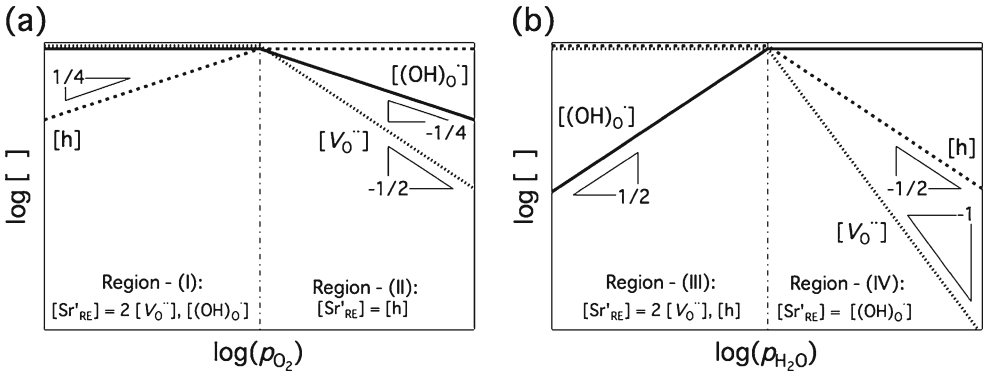

Fig. 1 Defect concentrations as functions of (**a**) oxygen partial pressure and (**b**) water vapor pressure.

$\sigma_h = \sigma_h^\circ$, hold. Then, when $[Sr'_{Nd}] = [(OH)_O^\bullet]$ holds, the relations, $\sigma_{O^{2-}} = \sigma^\circ_{O^{2-}} p_{H_2O}^{-1}$, $\sigma_{H^+} = \sigma^\circ_{H^+}$ and $\sigma_h = \sigma_h^\circ p_{O_2}^{\frac{1}{4}} p_{H_2O}^{-\frac{1}{2}}$, are expected. Figure 1 shows the Brouwer diagram constructed based on Eqs. (6), (8) and (9) with assuming $[O_O^\times] \approx 3$ in Eq. (10).

In this study, electrical conductivity measurements were carried out for $La_{1-x}Sr_xP_5O_{14-\delta}$ (x=0, 0.01, 0.03 and 0.05 in nominal formulae) and $(Nd_{1-x}Sr_x)_3PO_{7-\delta}$ (x=0 and 0.03). Major carriers in the above materials are identified based on the electrical conductivities as functions of water vapor, oxygen partial pressures and isotopic effect of hydrogen and deuteron on the electrical conductivity.

2 Experimental

Powders of ultraphosphates, $La_{1-x}Sr_xP_5O_{14-\delta}$ (x=0, 0.01, 0.03 and 0.05 in nominal), were prepared via the reported manner [38]. Appropriate amount of La_2O_3 (99.99 %, Rare Metallic Co., Ltd.) and $SrCO_3$ (99.99 %, Rare Metallic Co., Ltd.) were mixed together with twentyfold of phosphoric acid to metals in molar number ($P/(La + Sr) = 20$) in a gold crucible. Then, it was baked at 873 K or 973 K for 20 h in air. The resultant powders were filtered and well washed in distilled water with an ultrasonic washer in order to remove remaining phosphoric acid. Powders of $(Nd_{1-x}Sr_x)_3PO_7$ (x= 0 and 0.03) were prepared by a conventional solid state reaction route. Parts of the starting powders, $NdPO_4$ and $SrHPO_4$, were separately prepared by a precipitation method as in the literature [12, 13] prior to the solid state reaction. Starting powders of $NdPO_4$, $SrHPO_4$ and Nd_2O_3 were weighed in stoichiometric ratios and well mixed with a zirconia mortar and a zirconia pestle, and then, calcined at 1073–1673 K for 5–15 h. XRD (X-ray diffraction, M18X, Bruker AXS) measurements were carried out in order to check if the synthesized powders consisted of single phases.

The products were sintered in the form of disc using the SPS (Spark Plasma Sintering) equipment (Dr. Sinter Lab^{TM}, SPS Syntex Inc.). The pressure and the duration for the SPS were set to 30 MPa and 5 min, respectively, in the temperature ranges of 1223 K to 1278 K for $(La,Sr)P_5O_{14}$ and of 1723 K for $(Nd,Sr)_3PO_7$. Platinum was coated onto both surfaces of the specimens using an ion-coater (IB-5, Eiko Engineering Co., Ltd.) for $(La,Sr)P_5O_{14}$ while platinum paste was painted onto the surfaces of $(Nd,Sr)_3PO_7$ as electrodes for the electrical conductivity measurements. The cell was set to a single-chamber type apparatus as shown in Fig. 2. The specimen was sandwiched by porous Al_2O_3-plates with platinum mesh for current correction. Platinum lead wires, which were welded to platinum mesh, were connected to the sets of equipments (Electrochemical Interface SI1287 – Impedance/Gain-Phase Analyzer SI1260, Solartron Analytical or Potentiostat-Galvanostat 2000, Toho Technical Research – FRA 5095, NF Corporation) for ac impedance measurements. Since Al_2O_3-tube was connected to inner quartz tube by springs, the cell was kept under mechanical pressure to make sure the well-defined contact of current correctors with the electrodes.

For $(La,Sr)P_5O_{14}$, oxygen partial pressure dependence of the electrical conductivity was investigated in hydrogen partial pressure range of 1.0×10^{-2}–0.988 atm in the absence and the existence of water vapor with 1.2×10^{-2} atm at 523–673 K. In order to further investigate if the proton conducts in ceramics, the isotope effect of hydrogen and deuteron on the electrical conductivity was evaluated both in reducing gases such as 1.0×10^{-2} atm hydrogen/deuteron–1.2×10^{-2} atm water vapor/heavy water and in oxidizing gases

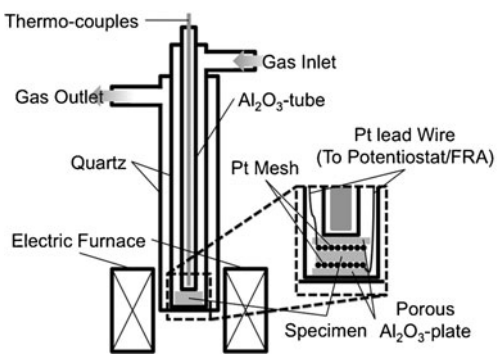

Fig. 2 A schematic illustration of an experimental setup for two-probe ac conductivity measurements

such as 1.0×10^{-2} atm oxygen–1.2×10^{-2} atm water vapor/heavy water. For $(Nd,Sr)_3PO_7$, the measurement were conducted at 873–1273 K in oxygen partial pressure range of 10^{-4}–1 atm in the absence and in the existence of water vapor with 1.9×10^{-2} atm.

3 Results and discussion

3.1 Specimens

Typical XRD patterns of the powders of ultraphosphates, $La_{1-x}Sr_xP_5O_{14-\delta}$ (x=0, 0.01, 0.03 and 0.05 in nominal), and oxyphosphates, $(Nd_{1-x}Sr_x)_3PO_{7-\delta}$ (x=0 and 0.03), are shown in Fig. 3. It was found from the figure that the powders prepared in the present study are well assigned to be the literature patterns of the lanthanum ultraphosphate [39] and the oxyphosphates both with a monoclinic structure [41]. This suggests that the products used in this study consisted of single phases. As results of SPS, the discs having the relative density of above 94.0 %, 96.2 % and 84.0 % for (La,Sr)$P_5O_{14-\delta}$, $(Nd_{0.97}Sr_{0.03})_3PO_{7-\delta}$, and Nd_3PO_7, respectively, were obtained.

3.2 Electrical conductivity of (La,Sr)P_5O_{14}

Figure 4 shows total conductivities in 1.0×10^{-2} atm hydrogen–1.2×10^{-2} atm water vapor at 673 K and 573 K as a function of strontium content, x. It was found that doping of Sr into La-site of the ultraphosphate enhanced the electrical conductivity more than half order of magnitude. It can be seen that the conductivity is independent of doping level, x, up to 5 mol%. Amezawa and his co-workers evaluated the electrical conductivity of $LaPO_4$ doped with alkaline earth metals. According to their report, when the nominal amount of dopant exceeds the solubility limit, the total conductivity saturates [21]. Thus, the saturation of the electrical conductivity with doping level, x, seen in Fig. 4, may be caused by the low solubility of Sr into La-site of LaP_5O_{14} such as at most 1 mol% although no extra peak was observed in XRD patterns as in Fig. 3. Thus, we will denote the doped lanthanum ultraphosphate composition as $La_{1-x}Sr_xP_5O_{14-\delta}$ for the following.

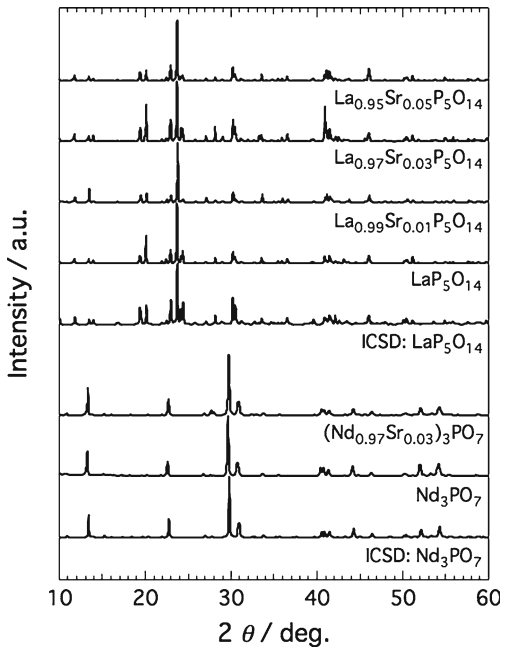

Fig. 3 XRD patterns of the powders of $La_{1-x}Sr_xP_5O_{14-\delta}$ (x=0, 0.01, 0.03 and 0.05 in nominal) and $(Nd_{1-x}Sr_x)_3PO_{7-\delta}$ (x=0 and 0.03). The patterns of LaP_5O_{14} [39] and Nd_3PO_7 [41], appearing in the literature, are also shown

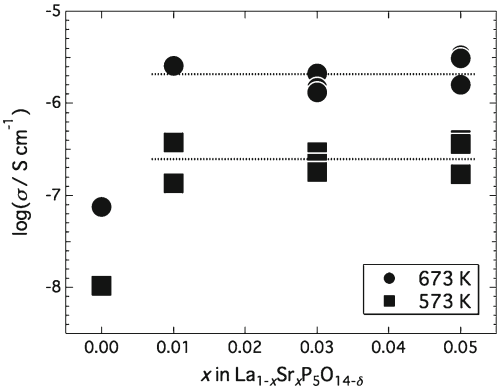

Fig. 4 The electrical conductivity of $La_{1-x}Sr_xP_5O_{14-\delta}$ as a function of the strontium content, x, in 1.0×10^{-2} atm hydrogen–1.2×10^{-2} atm water vapor at 573 K and 673 K

Figure 5 shows the electrical conductivity of $La_{1-x}Sr_xP_5O_{14-\delta}$ as a function of oxygen partial pressure at 573, 623 and 673 K. It was found that the electrical conductivity was independent of oxygen partial pressure in the oxygen partial pressure and temperature ranges investigated. This tendency is similar to the other phosphate based protonic conductors such as $La_{0.99}Sr_{0.01}PO_{4-\delta}$ [17] and $La_{0.97}Sr_{0.03}P_3O_{9-\delta}$ [19]. Figure 6 compares the electrical conductivities of $La_{1-x}Sr_xP_5O_{14-\delta}$ in 1.0×10^{-2} atm hydrogen–1.2×10^{-2} atm water vapor, unhumidified 1.0×10^{-2} atm oxygen and unhumidified 1.0×10^{-2} atm hydrogen as a function of inverse temperature. Both oxygen and hydrogen containing atmospheres, the electrical conductivity was found to be independent of water vapor pressure. This independency of the electrical conductivity on water vapor pressure is similar to $La_{0.97}Sr_{0.03}P_3O_{9-\delta}$ [19], while the electrical conductivity of $La_{0.99}Sr_{0.01}PO_{4-\delta}$ has a positive dependence of water vapor pressure both in hydrogen and oxygen containing environment [21].

In order to identify the predominant carrier in $La_{1-x}Sr_xP_5O_{14-\delta}$, isotope effect of hydrogen and deuterium on the electrical conductivity was investigated. Conductivities of $La_{0.99}Sr_{0.01}P_5O_{14-\delta}$ in reducing and oxidizing atmospheres

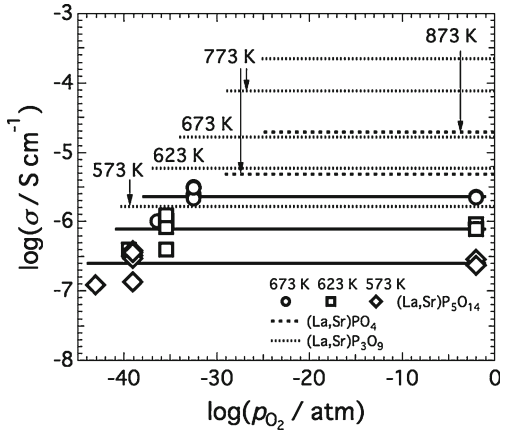

Fig. 5 The electrical conductivity of $La_{1-x}Sr_xP_5O_{14-\delta}$ as a function of oxygen partial pressure. The values of $La_{0.99}Sr_{0.01}PO_{4-\delta}$ [17] and $La_{0.97}Sr_{0.03}P_3O_{9-\delta}$ [19], appearing in the literatures, are also shown in the figure

are shown in Figs. 7 (a) and (b), respectively. As is seen in the figures, the conductivities in heavy water containing atmosphere decreased comparing with those in water containing atmosphere both in hydrogen and oxygen. The ratios of total conductivities, $\sigma_{H_2O}/\sigma_{D_2O}$, were found to be 1.16–1.24 and 1.14–1.22 in reducing and in oxidizing conditions, respectively, as shown in Fig. 7 (c). Since the electrical conductivity is independent of oxygen partial pressure in both hydrogen and oxygen as discussed above paragraph, the difference of the electrical conductivity, $\sigma_{H_2O}$and σ_{D_2O}, is surely caused by the isotopic effect of hydrogen and deuteron. The ratio of the electrical conductivities, $\sigma_{H_2O}/\sigma_{D_2O}$, are within the range expected in the case of the proton migration, explained as classical theory [45]. This suggests that the major carrier in $(La,Sr)P_5O_{14}$ is protons similar to the other phosphates [11–24, 26]. Therefore, $(La,Sr)P_5O_{14}$ as well as $(La,Sr)P_3O_9$ can be utilized in unhumidified environment as purely proton conducting electrolytes regardless of oxygen partial pressure.

Recent works by the first principles calculation on the defect structures in $(La,Sr)P_3O_9$ suggested that the oxygen deficit is formed by further condensation of (PO_4)-tetrahedra forming a $(PO_3)_n$ chain, resulting in significant lattice distortions. The hydration enthalpy of $(La,Sr)P_3O_9$ is comparatively negatively larger than those of oxides, suggesting that $(La,Sr)P_3O_9$ is likely to be hydrated even under low water vapor pressure [46, 47]. As a result, protonic defects, not oxygen deficits, compensates negatively charged defects, i.e. dopants in host sites, Sr'_{La}, contrary to rare-earth ortho-phosphates at high temperatures [10, 13, 17]. In $(La,Sr)P_5O_{14}$, the oxygen deficit is expected to be induced by further condensation of phosphate groups as in $(La,Sr)P_3O_9$. Independences of the proton conductivity on both oxygen and water vapor pressures suggest that the proton concentration in $(La,Sr)P_5O_{14}$ is fully saturated with ambient water vapor due to negatively large hydration enthalpy as in $(La,Sr)P_3O_9$ [46, 47]. The mechanisms of the oxygen deficit formation and the introduction of protonic defects in condensed phosphates are different from those of $(La,Sr)PO_4$ as in Eqs. (1) and (2).

3.3 Electrical conductivity of $(Nd,Sr)_3PO_7$

Figure 8 shows the electrical conductivity of $(Nd_{1-x}Sr_x)_3PO_{7-\delta}$ (x=0 and 0.03) as a function of inverse temperature in unhumidified 1.0×10^{-2} atm O_2 and 1.0×10^{-2} atm O_2–1.9×10^{-2} atm H_2O with open and closed symbols, respectively. The conductivity regarding $Nd_{0.99}Sr_{0.01}PO_{4-\delta}$ in unhumidified 1.0×10^{-2} atm O_2 and in 1.0×10^{-2} atm O_2–1.4×10^{-2} atm H_2O, evaluated by Kitamura and his co-workers [14], is shown in the figure. It was found that the conductivity of $(Nd_{0.97}Sr_{0.03})_3PO_{7-\delta}$ is larger than that of Nd_3PO_7 by one – half order of magnitude over the temperature range investigated. This suggests that doping of Sr into Nd-site of Nd_3PO_7 enhanced the electrical conductivity. It was also found that the electrical conductivity of $(Nd_{0.97}Sr_{0.03})_3PO_{7-\delta}$ considerably decreased by the introduction of water vapor. On the other hand, the electrical conductivity of non-dope Nd_3PO_7 was independent of water vapor pressure. This suggests that negative dependence of the electrical conductivity on water vapor pressure is caused by the doping of Sr into Nd-site. The difference of the electrical conductivity between in 1.0×10^{-2} atm O_2–1.9×10^{-2} atm H_2O and in unhumidified 1.0×10^{-2} atm O_2 is more visible as temperature decreased. The situation is the different from $Nd_{0.99}Sr_{0.01}PO_{4-\delta}$, i.e. increase of the total

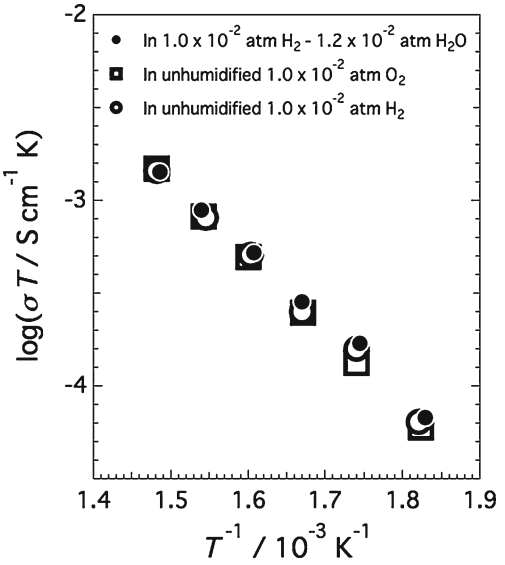

Fig. 6 The electrical conductivities of $La_{1-x}Sr_xP_5O_{14-\delta}$ in 1.0×10^{-2} atm hydrogen–1.2×10^{-2} atm water vapor, unhumidified 1.0×10^{-2} atm oxygen and unhumidified 1.0×10^{-2} atm hydrogen as a function of inverse temperature

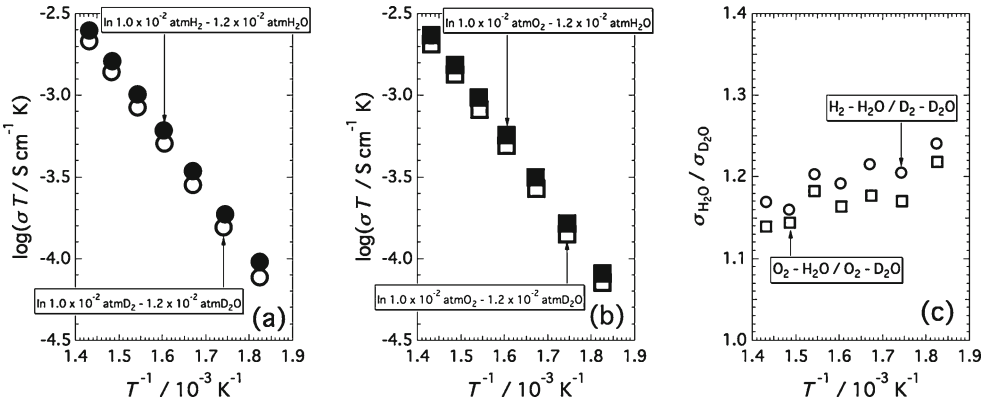

Fig. 7 Hydrogen and deuterium isotope effect on the total conductivities of $La_{1-x}Sr_xP_5O_{14-\delta}$ as functions of inverse temperature in (a) reducing and (b) oxidizing atmospheres. (c) Ratio of conductivities, $\sigma_{H_2O}/\sigma_{D_2O}$, in both reducing and oxidizing atmospheres

conductivity by increasing water vapor pressure [14], as shown in the figure. This suggests that the electrical conduction property in oxyphosphate is essentially different from the other phosphate-based protonic conductors.

Figure 9 shows the electrical conductivity of $(Nd_{0.97}Sr_{0.03})_3PO_{7-\delta}$ as a function of oxygen partial pressure in unhumidified and humidified oxygen at 973–1273 K. The electrical conductivity depended positively on oxygen partial pressure. A slope of $\log \sigma_{O^{2-}}$ vs. $\log p_{O_2}$ was close to 1/4 over the temperature and oxygen partial pressure ranges investigated. It was found that the electrical conductivity decreased by the introduction of water vapor. The decrease of the electrical conductivity was more remarkable as temperature and/or oxygen partial pressure decreased.

According to Brouwer Diagram shown in Fig. 1, only the electron hole can have a positive dependence on oxygen partial pressure with a factor of 1/4 under the charge neutrality conditions, $[Sr'_{Nd}] = 2[V_O^{\bullet\bullet}]$ or $[Sr'_{Nd}] = [(OH)_O^{\bullet}]$. In the case of the former condition, protons have positive dependence on water vapor pressure with a factor of 1/2 and electron hole is expected to be independent of water vapor pressure. This means, water vapor pressure dependence of the electrical conductivity cannot be explained under the condition, $[Sr'_{Nd}] = 2[V_O^{\bullet\bullet}]$, under the assumption that the mobility is independent of gas partial pressure. On the other hand, in the case of the latter charge neutrality condition, both oxygen deficit and electron hole have negative dependence on water vapor pressure by factors of −1 and −1/2, respectively, which is in consistent with the gas partial pressure dependences of the electrical conductivity as in Fig. 9. As in Fig. 9, the electrical conductivity decreased by the introduction of water vapor, the partial protonic conductivity is expected to be smaller than other possible carriers such as oxygen deficit and electron hole. Thus, the following relation is expected to hold,

$$\sigma = \sigma^{\circ}_{O^{2-}} p_{H_2O}^{-1} + \sigma^{\circ}_{h} p_{O_2}^{\frac{1}{4}} p_{H_2O}^{-\frac{1}{2}} \quad (12)$$

Figure 10 simulates the total conductivity, partial conductivities of oxide ion and electron hole under the assumption that $\sigma^{\circ}_{O^{2-}}/\sigma^{\circ}_{h}$ in case-(1) >> $\sigma^{\circ}_{O^{2-}}/\sigma^{\circ}_{h}$ in case-(2) based on Eq. (12). When the contributions of oxide ion and electron hole is comparable, the gradient of log σ – log

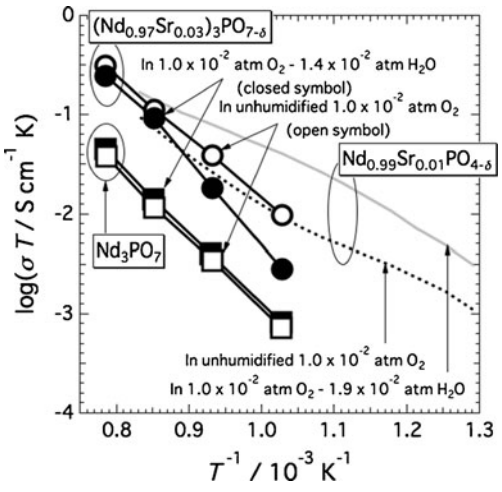

Fig. 8 The electrical conductivities of $(Nd_{1-x}Sr_x)_3PO_{7-\delta}$ (x=0 and 0.03) as a function of inverse temperature in oxygen containing atmospheres. Solid and broken curves represent the electrical conductivities of $Nd_{0.99}Sr_{0.01}PO_{4-\delta}$ in 1.0×10^{-2} atm oxygen–1.4×10^{-2} atm water vapor and in unhumidified 1.0×10^{-2} atm oxygen [14]

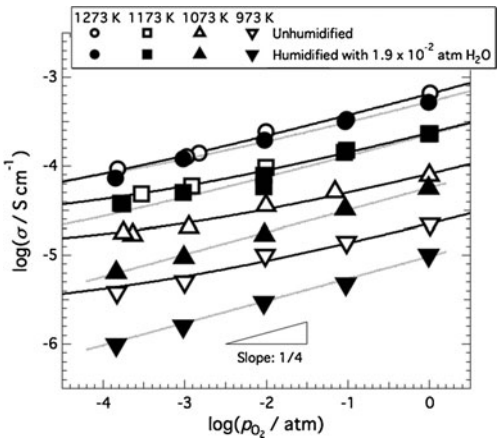

Fig. 9 The electrical conductivity of $(Nd_{0.97}Sr_{0.03})_3PO_{7-\delta}$ as a function of oxygen partial pressure

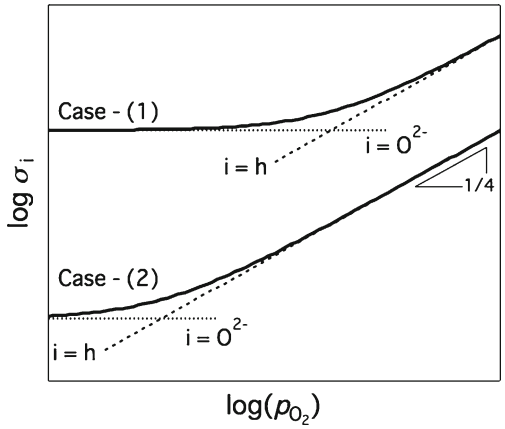

Fig. 10 Simulated total conductivity, partial conductivities of oxide ion and electron hole as a function of oxygen partial pressure for two-cases based on Eq. (12). $\sigma^{\circ}_{O^{2-}}/\sigma^{\circ}_{H^{+}}$ in case-(1) >> $\sigma^{\circ}_{O^{2-}}/\sigma^{\circ}_{H^{+}}$ in case-(2) was assumed to draw the figure

p_{O_2} relation will have 0–1/4 under constant partial pressure of water vapor. The comparative region of the partial conductivity contributions of oxide ion and electron hole is expected to shift to lower oxygen partial pressure range when higher pressure of water vapor is introduced in the gas phase. As shown in Fig. 9, at a constant temperature typically 973 and 1073 K, the gradient of log σ – log p_{O_2} became close to 1/4 by introduction of water vapor, suggesting that the major carrier changed from the mixture of oxide ion and electron hole to electron hole. The gradient of log σ – log p_{O_2} became close to 1/4 both in humidified and unhumidified gases as temperature decreased. Increase of the gradient by decreasing the temperature may be due to the difference in activation energy between oxide ion and electron hole. The oxide ion have higher activation energy than that of electron hole, the contribution of electron hole conductivity became remarkable as temperature decreased, resulting in the increase of the log σ – log p_{O_2} slope toward 1/4.

Similar to the case of the other phosphate based protonic conductors, the significant concentration of protonic defect is induced in $(Nd_{0.97}Sr_{0.03})_3PO_{7-\delta}$. However, attributed to the small proton mobility to the other carriers such as oxide ion and electron hole, the contribution of proton conductivity is negligible.

3.4 Comparison of conductivities among phosphates

Figure 11 compares the conductivities of the various phosphates such as $(La,Sr)PO_4$ [13], $(Nd,Sr)PO_4$ [14], $(La,Sr)P_3O_9$ [19], $(La,Sr)_7P_3O_{18}$ [16], polycrystalline $(La,Sr)P_5O_{14}$ and $(Nd,Sr)_3PO_7$ in humidified environments. The electrical conductivity of a single crystal of $(La,Sr)P_5O_{14}$ [26] is also provided in the figure.

In the case of the phosphates having protonic conductivity, the gradient of conductivity over the inverse temperature becomes small as temperature increased. Thus, the activation energy of proton migration was evaluated by the electrical conductivity in the lower temperature region. The activation energy of protonic conduction in $La_{1-x}Sr_xP_5O_{14-\delta}$ was evaluated to be 76 kJ mol^{-1}, which is comparable to the other phosphate based protonic conductors. The phosphates except for oxyphosphate had the activation energies of 77–82 kJ mol^{-1}, which is similar value of doped LaP_3O_9 (74 kJ mol^{-1} [23]) and doped ZrP_2O_7 (68–76 kJ mol^{-1} [24]) by Nalini et al., and single crystal of doped LaP_5O_{14} (73–86 kJ mol^{-1} [26]). $La_{1-x}Sr_xP_5O_{14-\delta}$ had comparative protonic conductivity to the other phosphate based protonic conductors as well as single crystal $La_{0.95}Sr_{0.05}P_5O_{14-\delta}$ [26].

However, the situation seems to be different for oxyphosphate, $(Nd_{0.97}Sr_{0.03})_3PO_7$. As shown in Fig. 11, the oxyphosphate had apparent activation energy of 165 kJ mol^{-1}, which is far larger than the above phosphate based protonic conductors. This may be attributed to the difference in defect structures and carriers in the oxyphosphate.

4 Conclusions

The electrical conductivities of $La_{1-x}Sr_xP_5O_{14-\delta}$ (x is at most 0.01) and $(Nd_{0.97}Sr_{0.03})_3PO_{7-\delta}$ were investigated in this study. Protonic defects are induced in both ceramics in

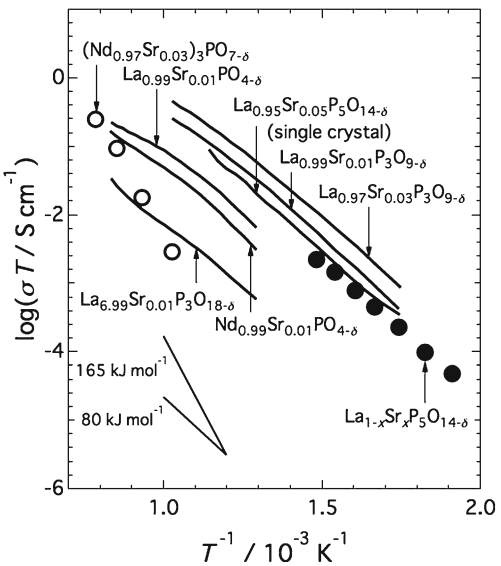

Fig. 11 Summary of the conductivities of the phosphates as a function of inverse temperature. The conductivities of $La_{1-x}Sr_xP_5O_{14-\delta}$ (in 1.0×10^{-2} atm H_2–1.2×10^{-2} atm H_2O) and $(Nd_{0.97}Sr_{0.03})_3PO_{7-\delta}$ (in 1.0×10^{-2} atm O_2–1.4×10^{-2} atm H_2O) were revealed in this study. The electrical conductivities of $La_{0.99}Sr_{0.01}PO_{4-\delta}$ (in 1.0×10^{-2} atm H_2–1.4×10^{-2} atm H_2O) [7], $La_{0.99}Sr_{0.01}P_3O_{9-\delta}$ and $La_{0.97}Sr_{0.03}P_3O_{9-\delta}$ (both in 3.0×10^{-2} atm H_2–1.4×10^{-2} atm H_2O) [18], single crystal of $La_{0.95}Sr_{0.05}P_5O_{14-\delta}$ [26], $La_{6.99}Sr_{0.01}P_3O_{18-\delta}$ (in 1.0×10^{-2} atm O_2–1.4×10^{-2} atm H_2O) [13] and $Nd_{0.99}Sr_{0.01}PO_{4-\delta}$ (in 1.0×10^{-2} atm O_2–1.4×10^{-2} atm H_2O) [10] were also shown in the figure

humidified environment. $La_{1-x}Sr_xP_5O_{14-\delta}$ had considerable protonic conductivity such as 4.7×10^{-5}–2.2×10^{-3} S cm^{-1} in the temperature range of 523–673 K. The activation energy was evaluated to be 76 kJ mol^{-1}. Independencies of the protonic conductivity on both partial pressures of water vapor and oxygen suggest that the ceramics is utilized as purely proton conducting electrolytes even in unhumidified environment. The protonic conductivity and the activation energies are similar to the other phosphate-based protonic conductors. For the phosphates having condensed phosphate ions such as $(La,Sr)P_3O_9$ and $(La,Sr)P_5O_{14}$, protonic defects compensates the negative defects, Sr'_{La}. Thus, $(La,Sr)P_3O_9$ and $(La,Sr)P_5O_{14}$ are expected to be used as electrolytes even in unhumidified environment. For $(Nd_{0.97}Sr_{0.03})_3PO_{7-\delta}$, attributed to small contribution of protonic conductivity, the major carrier was identified to be a mixture of oxide ion and electron hole in unhumidified environment in the temperature range of 973–1273 K and humidified gas at temperatures above 1173 K. It turns to be only electron hole at temperatures below 1073 K in humidified oxygen. The origin of the trend is needed to be further investigated in the future work.

Acknowledgments This study was supported by the JFE 21st Century Foundation, Toyota Motor Co., Ltd. and the Grant-in-Aid for JSPS (Japan Society of the Promotion of Science) Fellows from the Ministry of Education, Culture, Sports, Science and Technology of Japan.

References

1. H. Iwahara, T. Esaka, H. Uchida, N. Maeda, Solid State Ionics. **3** (4), 359 (1981)
2. K.D. Kreuer, Annu. Rev. Mater. Res. **33**, 333 (2003)
3. H. Iwahara, Solid State Ionics. **77**, 289 (1995)
4. H. Iwahara, Solid State Ionics. **86–88**, 9 (1996)
5. T. Schober, Solid State Ionics **162–163**, 277 (2003)
6. N. Ito, M. Iijima, K. Kimura, S. Iguchi, J. Power Source. **152**, 200 (2005)
7. H. Matsumoto, I. Nomura, S. Okada, T. Ishihara, Solid State Ionics. **179**, 1486–1489 (2008)
8. D. Lybye, N. Bonanos, Solid State Ionics. **125**, 339 (1999)
9. J. Han, Z. Wen, J. Zhang, B. Lin, X. Wu, J. Electroceram. **22**, 20 (2009)
10. H. Kato, H. Yugami, J. Electroceram. **18**, 219 (2007)
11. T. Norby, N. Christiansen, Solid State Ionics. **77**, 240 (1995)
12. K. Amezawa, S. Kjelstrup, T. Norby, Y. Ito, J. Electrochem. Soc. **145**, 3313 (1998)
13. K. Amezawa, H. Maekawa, Y. Tomii, N. Yamamoto, Solid State Ionics. **145**, 233 (2001)
14. N. Kitamura, K. Amezawa, Y. Tomii, N. Yamamoto, Solid State Ionics **162**, 161 (2003)
15. K. Amezawa, Y. Kitajima, Y. Tomii, N. Yamamoto, Electrochem. Solid St. **7**, A511 (2004)
16. K. Amezawa, Y. Tomii, N. Yamamoto, Solid State Ionics. **175**, 569 (2004)
17. K. Amezawa, Y. Tomii, N. Yamamoto, Solid State Ionics. **176**, 135 (2005)
18. K. Amezawa, Y. Kitajima, Y. Tomii, N. Yamamoto, M. Wideroe, T. Norby, Solid State Ionics. **176**, 2867 (2005)
19. K. Amezawa, Y. Uchimoto, Y. Tomii, Solid State Ionics. **177**, 2407 (2006)
20. N. Kitamura, K. Amezawa, Y. Uchimoto, Y. Tomii, T. Hanada, N. Yamamoto, Solid State Ionics. **177**, 2369 (2006)
21. K. Amezawa, Y. Tomii, N. Yamamoto, Solid State Ionics. **176**, 143 (2005)
22. K. Amezawa, Y. Nishikawa, Y. Tomii, N. Yamamoto, J. Electrochem. Soc. **152**, A1060 (2005)
23. V. Nalini, R. Haugsrud, T. Norby, Solid State Ionics. **181**, 1264 (2010)
24. V. Nalini, K. Amezawa, W. Xing, T. Norby, J. Electrochem. Soc. **157**, B1491 (2010)
25. I. Hammas, K. Horchani-Naifer, M. Férid, J. Rare Earth. **28**, 321 (2010)
26. S.R. Phadke, J.C. Nino, J. Am. Ceram. Soc. **94**, 1817 (2011)
27. K. Amezawa, N. Takahashi, N. Kitamura, Y. Tomii, N. Yamamoto, Solid State Ionics. **175**, 575 (2004)
28. R. Haugsrud, T. Norby, Nature Mat. **5**, 193 (2006)
29. F.A. Kröger, H.J. Vink, in *Solid state physics, vol. 3*, ed. by F. Steitz, D. Turnbull (Academic, New York, 1956)
30. S. Gopalan, A.V. Virkar, J. Electrochem. Soc. **140**, 1060 (1993)
31. M.J. Scholten, J. Schoonman, J.C. van Miltenburg, H.A.J. Oonk, Solid State Ionics. **61**, 83 (1993)
32. N. Bonanos, K.S. Knight, B. Ellis, Solid State Ionics. **79**, 161 (1995)
33. K.D. Kreuer, Solid State Ionics. **97**, 1 (1997)
34. H. Matsumoto, S. Okada, S. Hashimoto, K. Sasaki, R. Yamamoto, M. Enoki, T. Ishihara, Ionics **13**, 93 (2007)
35. H. Matsumoto, Y. Kawasaki, N. Ito, M. Enoki, T. Ishihara, Electrochem. Solid-St. **10**, B77 (2007)
36. L. Niinisto, M. Keskela, in *Handbook on the physics and chemistry of rare earths*, ed. by K.A. Gschneidner Jr., L. Eyring, vol. 9 (Elsevier, Amsterdam, 1987)
37. M.S. Wong, E.R. Kreidler, J. Am. Ceram. Soc. **70**, 396 (1987)
38. M. Tsuhako, S. Ikeuchi, T. Matsuo, I. Motooka, M. Kobayashi, Bull. Chem. Soc. Jpn. **52**, 1034 (1979)
39. ICSD #411260: J.M. Cole, M.R. Lees, J.A.K. Howard, R.J. Newport, G.A. Saunders, E. Schonherr, J. Solid State Chem. **150**, 377 (2000)
40. E.G. Tselebrovskaya, B.F. Dzhurinskii, O.I. Lyamina, Inorg. Mater. **32**, 52 (1997)
41. ICSD#82718: K. K. Doklady, N. E. Kuz'mina, B. F. Dzhurinskii, E. G. Tselebrovskaya, Doklady Akad. Nauk. **341**, 644 (1995)
42. S. Ku, J. Zhang, J. Lumin. **122–123**, 500 (2007)
43. Y. Jin, W. Qin, J. Zhang, Y. Wang, C. Cao, J. Zhang, X. Ren, G. Wang, G. Wei, L. Wang, L. Jin, P. Zhu, Mater. Lett. **62**, 3146 (2008)
44. J. Zhang, S. Lu, J. Nanosci. Nanotech. **8**, 1410 (2008)
45. A.S. Nowich, A.V. Vaysleyb, Solid State Ionics. **97**, 17 (1997)
46. K. Amezawa, H. Takahashi, A. Kuwabara, A. Unemoto, T. Kawada, Int. J. Hydrogen Energ. 37 (2012) 7995-8003.
47. H. Takahashi, Master's Thesis (2011), Tohoku University.